



# Segmentation of Pathologic Hearts in Long-Axis Late-Enhancement MRI

Cybèle Ciofolo and Maxim Fradkin

Medisys Research Lab, Philips Healthcare, Suresnes, France  
cybele.ciofolo@philips.com.

**Abstract.** We propose a new method to segment long-axis cardiac MR images acquired with a late-enhancement protocol. Detecting the myocardium boundaries is difficult in these images because healthy myocardium appears dark while the intensity of enhanced areas ranges from gray to white, depending on the myocardial damage. In this context, geometrical template deformation, alternated with the update of a damaged tissue map, allows us to include abnormal myocardium parts in the final segmentation. The template and map are initialized using short-axis images and the deformation parameters are adapted according to the type of enhancement pattern. Good segmentation results are obtained on a database of real pathologic heart images presenting various types of abnormal myocardium tissues.

## 1 Introduction

Viability assessment is nowadays an unavoidable part of cardiac examinations, used for both surgery and therapy planning. In particular, the proportion of viable myocardium is a major factor in determining whether a patient may benefit from revascularization. In order to locate and quantify the extent of abnormal myocardial tissues, clinicians generally use late-enhancement cardiac magnetic resonance (LE CMR) images, which are acquired around twenty minutes after contrast agent injection. At the LE CMR acquisition time, due to the loss of membrane integrity in damaged tissues, the contrast agent accumulates in abnormal parts of the myocardium, which are consequently enhanced (become bright) while healthy myocardium remains dark, as shown in Fig. 1. Although short-axis (SA) slices are useful to have a global estimation of the damaged tissues position in the left ventricle, they are generally acquired with poor resolution along the ventricle long axis (around 5 to 10mm). Long-axis (LA) images (2 chambers and 4 chambers views) consequently bring useful additional information to viability studies, especially concerning the apical area.

Many publications and commercial products propose automatic or semi-automatic methods to segment the left ventricle in CMR images. However, most of them, involving shape and appearance models [1, 2], deformable meshes [2], level sets [3, 4] or graph-cuts [5] relate to functional (or cine) images, in which there is no enhanced area in the myocardium. As for late-enhancement acquisitions, in addition to semi-automatic approaches, generally used to delineate the

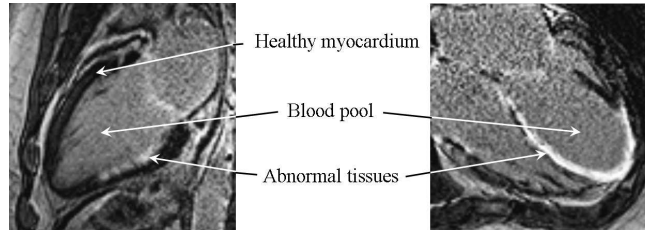


**Fig. 1.** Examples of long-axis late-enhancement images of pathologic hearts.

myocardium contours in SA images [6, 7], one automatic segmentation algorithm was published by Dikici et. al. [8] and more recently, we also proposed a new automatic approach [9]. But to the best of our knowledge, no method has yet been reported for segmenting LE LA images, which is the objective of this work.

The main difficulty with processing LE CMR data is the non-homogeneous intensity of the myocardium resulting from contrast agent accumulation in abnormal tissues, which leads to various enhanced patterns, depending on the myocardial damage. Moreover, contrary to SA images, no ring shape prior can be used to segment the myocardium in LA images. In this work, we present an iterative algorithm which alternates the deformation of a geometrical template toward the myocardium boundaries and the update of a damaged tissue map to guide the deformation. This is done automatically, except for a one-time user choice which specifies the enhancement pattern among four pre-defined ones.

This paper is organized as follows: the myocardium segmentation method is presented in Section 2 and quantitatively assessed in Section 3, then we conclude in Section 4.

## 2 Method

This section describes the main features of our algorithm: the deformable template representing the myocardium, the associated binary map of abnormal tissues and the iterative workflow which leads to the final segmentation.

### 2.1 Deformable template

**Template description.** The myocardium is modelled as a closed ribbon structure with an imaginary centerline  $C(s) = (x(s), y(s))$  and a variable width  $w(s)$ , both of which are continuous spline interpolations of a discrete set of  $\{p_k = (x_k, y_k, w_k)\}$  samples defined at each node (see Fig. 2). This compact representation provides a natural coupling between the endocardium  $C_i$  and the epicardium  $C_o$  (the inside and outside contours). We also define the two regions  $\mathcal{M}$  and  $\mathcal{B}$ , corresponding respectively to the myocardium and blood pool, as shown in Fig. 2.

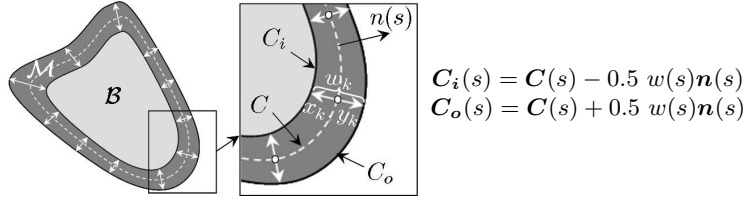


**Fig. 2.** Template geometry (left); Detailed zoom (center).

**Template deformation.** We aim at finding the set of parameters minimizing a criterion that expresses the match of the template and the image evidence, given some prior knowledge. Built from observations of typical cardiac images, this knowledge is translated into mathematical terms expressing shape, contour and region constraints. In the remainder,  $I$  is the image and the  $\lambda_i$ 's are scalar weights balancing the various terms. Let  $\mathbf{p} = \{p_k = (x_k, y_k, w_k)^T, k \in \llbracket 1, N \rrbracket\}$  be our parametric model. The problem can now be formalized as follows:

$$\min_{\mathbf{p}} \left\{ F(\mathbf{p}, I) = \underbrace{F_s(\mathbf{C}, w)}_{\text{shape}} + \underbrace{F_c(\mathbf{C}_i, \mathbf{C}_o, I)}_{\text{contour}} + \underbrace{F_r(\mathcal{M}, \mathcal{B}, I)}_{\text{region}} \right\}$$

*Shape:* the first part of this term constraints the template curve shape to be affinely similar with a pre-defined shape  $\tilde{\mathbf{C}}$ . It is defined as the error of the best affine transformation  $T$  between the current contour  $\mathbf{C}$  and a pre-defined contour  $\tilde{\mathbf{C}}$ . The second part is a regularity constraint on the template width variation:

$$F_s(\mathbf{C}, w) = \lambda_0 \int_0^1 |\mathbf{C}(s) - T(\tilde{\mathbf{C}}(s))|^2 ds + \lambda_1 \int_0^1 |w'(s)|^2 ds.$$

At the beginning of the segmentation,  $\tilde{\mathbf{C}}$  is the initial template. During the segmentation process, it is updated as explained in the segmentation workflow described in Section 2.3, and set equal to the most recent template shape, which is more reliable than the initial one. One particular advantage of this similarity term is to softly constrain the valve plane shape and curvature.

*Contour:* The endocardium and the epicardium walls are preferred locations of image gradients, as expressed by:

$$F_c(\mathbf{C}_i, \mathbf{C}_o, I) = \lambda_2 \int_0^1 \nabla I_{in}(s) ds - \lambda_3 \int_0^1 |\nabla I_{on}(s)| ds,$$

where  $\nabla I_{in} = \nabla I(\mathbf{C}_i(s)) \cdot \mathbf{n}(s)$  (respectively  $\nabla I_{on}$  with  $\mathbf{C}_o$ ),  $\nabla I$  is the image gradient and  $\mathbf{n}(s)$  is the outward-pointing normal to the centerline. To implement this term, we use gradient filters that express prior knowledge on the relative intensity of normal and abnormal parts of the myocardium, as explained in the *Special processing for abnormal tissues* paragraph below.

*Region.* The blood pool gray levels should be homogeneously distributed. Also, normal myocardium tissues are dark while abnormal ones are bright, which results in a strong global contrast with the blood pool. Therefore we have:

$$F_r(\mathcal{M}, \mathcal{B}, I) = \frac{\lambda_4}{|\mathcal{M}|} \int_{\mathcal{M}} |I(x, y) - \bar{m}| dx dy + \frac{\lambda_5}{|\mathcal{B}|} \int_{\mathcal{B}} |I(x, y) - \bar{b}| dx dy + \lambda_6(\bar{m} - \bar{b}),$$

where region  $\mathcal{B}$  has an average intensity  $\bar{b}$  and area  $|\mathcal{B}|$ , while the expected intensity is  $\bar{m}$  for the myocardium region  $\mathcal{M}$ .

**Special processing for abnormal tissues.** As mentioned earlier, the intensities of abnormal myocardial parts differ from those of healthy regions, which implies some adaptation of the criterion terms. Abnormal areas are detected with a map of abnormal tissues that is computed and updated during the segmentation process, as explained in Section 2.2. If the detection is positive, as damaged myocardium is brighter than the surrounding organs, the gradient filters defining the expected contrast along the borders are inverted. For the same reason, the expected value inside the myocardium  $\bar{m}$  (used in  $F_r$ ) is the maximum value of the intensity range instead of the minimum value for healthy myocardium. Let us note that these extremal values are not *ad hoc* parameters but come from the acquisition parameters of real LE CMR images, which are tuned so that the healthy myocardium appears as dark as possible and scars as bright as possible.

**Initialization.** Correctly positioning the geometrical template with no prior information concerning damaged tissues is very difficult, especially if large parts of the myocardium are enhanced. For this reason, the template is initialized using the segmentation result that is automatically obtained in the SA images acquired in the same examination as the LA views [9]. The SA result consists in two 3D meshes representing the inner and outer myocardium walls in the stack of SA images. To initialize the template position, we compute the intersection between the meshes, the SA slices and the LA plane. This results in pairs of points (endocardium and epicardium) sampled along the myocardium (Fig. 3(a-b)). However, SA and LA images being acquired at different breatholds, they are slightly misaligned and the intersections can be used for initialization only. Each pair of points then defines the template width associated to a node initially positioned at the center of the pair. As the SA slices do not intersect the left ventricle apical area, an additional node is computed by extrapolation:  $\mathbf{x}_{p_a} = \frac{1}{2}(\mathbf{x}_{p_0} + \mathbf{x}_{p_1}) + ((\mathbf{x}_{p_0} - \mathbf{x}_{p_2}) + (\mathbf{x}_{p_1} - \mathbf{x}_{p_3}))$ , where  $\mathbf{x}_{p_i}$  is the position vector of the node  $p_i$ , whose location on the template is shown in Fig. 3(c). The width associated to the extrapolated  $p_a$  node is the average width computed over all the other nodes. Finally, the centerline is interpolated from the nodes position and the nodes are equally resampled to obtain the initial template (Fig. 3(d)).

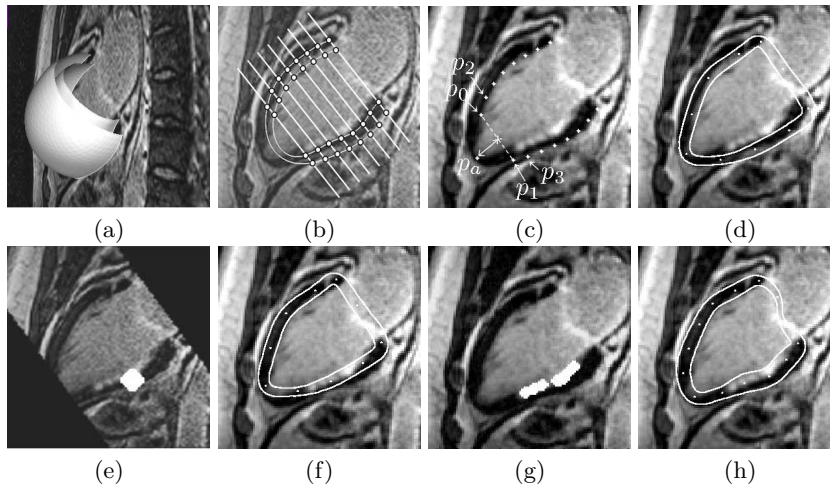


**Fig. 3.** (a)-(b) Intersection of SA meshes with SA slices and LA plane; (c) Initial position of the template nodes; (d) Initial template; (e) Initial map of abnormal tissues based on SA meshes, with black areas corresponding to regions not covered by the SA slices, where no information is available; (f) Coarse segmentation based on initial map; (g) Updated map of abnormal tissues; (h) Final result based on updated map.

**Optimization.** We use a *greedy* optimization scheme [10] embedded in a coarse-to-fine approach to simultaneously optimize the nodes position and ribbon width.

## 2.2 Map of abnormal tissues

**Map description.** The map of abnormal tissues is a binary 2D image with the same dimensions as the LA image, whose non-zero pixels indicate the location of likely abnormal tissues. Examples of such maps superimposed on the LA image are shown in Fig. 3(e) and Fig. 3(g).

**Map initialization.** The organs surrounding the myocardium constitute a textured background, which makes the detection of abnormal tissues very difficult if no prior information about the left ventricle boundaries is provided at the beginning of the segmentation process. Consequently, the 3D meshes resulting from SA segmentation are used once again. More precisely, our SA automatic algorithm detects abnormal tissues by comparison with the mean blood pool intensity and labels the corresponding vertices in the 3D meshes. Among these vertices, the closest to the LA plane are projected onto it. Simple morphological operations (closing and dilation) applied on the projected labels lead to the initial map of abnormal tissues (Fig. 3(e)).

**Map update.** After the first (or coarse) segmentation operation, the map is updated using the current position of the template contours. First, an area of interest is defined along the centerline. This area has to be large enough in the blood pool direction to include subendocardial scars. Then, a thresholding followed by morphological closing and dilation are done in the area of interest to obtain a new map with large “likely abnormal tissues” areas (Fig. 3(g)).

### 2.3 Segmentation workflow

The segmentation is done with the following succession of operations:

1. *Fully automatic segmentation of SA views* (Result visible in Fig. 3(a));
2. *Initialization of the geometrical template position* (Fig. 3(b-d));
3. *Initial map of abnormal tissues estimation* (Fig. 3(e));
4. *Coarse deformation of the geometrical template* (Fig. 3(f)): at this stage, as the initial map may not include all abnormal tissues, the segmentation is difficult for images presenting large transmural scars (see Fig. 4(b)). A strong weight is consequently given to the shape term to avoid large deformations around damaged areas;
5. *Update of both the map of abnormal tissues and  $\tilde{C}$  contour* (Fig. 3(g));
6. *Fine deformation of the geometrical template according to the updated map* (Fig. 3(h)): the map is now more reliable and the shape constraint is relaxed. Stronger and lower weights are given respectively to the homogeneity and contour terms, which allows the final contours to enclose damaged areas.

Four sets of deformation parameters are pre-defined, corresponding to the type of damaged tissues: large transmural scar, sub-endocardial scar, diffuse or small enhanced areas and no visible scar. At the beginning of the segmentation process, one single choice is required from the user to select one of these four abnormality types. This is the only user interaction that is used in this algorithm.

## 3 Results

We quantitatively assessed the performance of the method on a database of 20 LE CMR LA acquisitions of  $256 \times 256$  pixels, with a pixel size of 1.5mm, containing various types of abnormal tissues (large white transmural scars, sub-endocardial scars, scattered white areas...). Three skilled operators provided manual contours for comparison with our segmentation algorithm.

**Qualitative results.** The myocardium is well segmented in all images, as shown in Fig. 4. The scar map and the decrease of the contrast constraint in the contour term during the fine segmentation phase allow the contours to enclose sub-endocardial scars (Fig. 4(a) and 4(c)). This is of critical importance to compute clinical parameters such as the transmural extent of myocardial damage, generally expressed as a percentage (25%, 50%, 75% or 100%) of the myocardium width. On the other hand, this may induce slight inaccuracies along

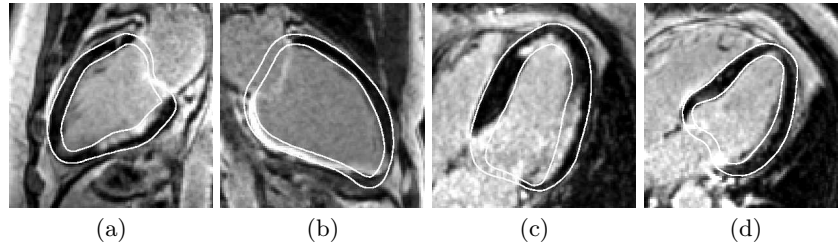


**Fig. 4.** Examples of segmentation results with various enhancement patterns. (a) Sub-endocardial scar; (b) Large transmural scar; (c) Several sub-endocardial scars; (d) Fuzzy endocardium boundary.

fuzzy boundaries, especially around the papillary muscles (Fig. 4(d)) or along the valve plane. However, this does not affect the damage areas and the related clinical parameters, it is thus considered as acceptable.

**Quantitative assessment.** The distance between contours segmented with our algorithm and contours drawn by each of the three experts is computed after exclusion of the valve plane area: the manual contours are drawn so that the valve plane is defined by a straight line and all the points above this line are automatically excluded from all contours. The mean distance values are summarized in Table 1, as well as the mean distance between each manual contour and the same contour drawn by the two other operators, which illustrates inter-observer variability.

The mean positioning error is around 1.5 pixels, which is a reasonable result to compute viability parameters, given that the inter-observer variability is around or higher than 1 pixel, depending on the contour. Let us note that these variability values are larger than those observed in functional (cine) images [11], showing that the segmentation of LE CMR data is particularly challenging. Also, the areas where larger errors occur correspond to areas with larger inter-observer variability, such as fuzzy boundary regions like low-contrasted scars, around the papillary muscles or regions close to the valve plane.

Finally, the LA segmentation takes 7 seconds in average with a 3.19GHz PC.

Contour	Unit	$D_{Ref1}$	$D_{Ref2}$	$D_{Ref3}$	Variability
Endocardium	mm	$2.4 \pm 0.9$	$2.6 \pm 0.9$	$2.3 \pm 0.8$	$1.7 \pm 0.7$
	pixels	$1.6 \pm 0.6$	$1.7 \pm 0.6$	$1.5 \pm 0.5$	$1.1 \pm 0.5$
Epicardium	mm	$2.3 \pm 1.0$	$2.4 \pm 0.9$	$2.4 \pm 1.1$	$1.5 \pm 0.9$
	pixels	$1.5 \pm 0.6$	$1.6 \pm 0.6$	$1.6 \pm 0.7$	$1.0 \pm 0.6$

**Table 1.** Mean distance  $D$  (in millimeters and pixels) to manual contours drawn by 3 human observers ( $Ref1$  to  $Ref3$ ) and inter-observer variability

## 4 Conclusion

We proposed a new method to delineate myocardial contours in long-axis late-enhancement images with a minimal user interaction, using a deformable template and binary scar maps. The quantitative evaluation showed that the obtained contours are accurately positioned and are eligible to automatically compute clinical parameters, such as the transmural extent of myocardial scar following heart infarct.

## 5 Acknowledgments

We are grateful to Benoît Mory from the Medisys Research Lab of Philips Healthcare for helping us in designing the deformable template and associated optimization scheme. We also would like to thank Gilion Hautvast and Marcel Breeuwer from Philips Healthcare — The Netherlands for fruitful discussions, active participation in programming and providing us with images and manual contours.

## References

1. Mitchell, S.C. et al.: Multistage hybrid active appearance model matching: segmentation of left and right ventricles in cardiac MR images. *IEEE Trans. Med. Imag.* **20**(5) (2001) 415–423
2. Kaus, M.R. et al.: Automated segmentation of the left ventricle in cardiac MRI. *Medical Image Analysis* **8**(3) (2004) 245–254
3. Niessen, W.J. et al.: Geodesic deformable models for medical image analysis. *IEEE Trans. Med. Imag.* **17**(4) (1998) 634–641
4. Paragios, N.: A variational approach for the segmentation of the left ventricle in cardiac image analysis. *International Journal of Computer Vision* **50**(3) (2002) 345–362
5. Jolly, M.P.: Automatic segmentation of the left ventricle in cardiac MR and CT images. *International Journal of Computer Vision* **70**(2) (2006) 151–163
6. Noble, N.M.I. et al.: The automatic identification of hibernating myocardium. In: 7th International Conference on Medical Image Computing and Computer-Assisted Intervention (MICCAI). (2004) 890–898
7. Heiberg, E. et al.: Semi-automatic quantification of myocardial infarction from delayed contrast enhanced magnetic resonance imaging. *Scandinavian Cardiovascular Journal* **39**(5) (2005) 267–275
8. Dikici, E. et al.: Quantification of delayed enhancement MR images. In: 7th International Conference on Medical Image Computing and Computer-Assisted Intervention (MICCAI). (2004) 250–257
9. Ciofolo, C. et al.: Automatic myocardium segmentation in late-enhancement MRI. In: *IEEE International Symposium on Biomedical Imaging: From Nano to Macro (ISBI)*. (2008)
10. Williams, D.J., Shah, M.: A fast algorithm for active contours and curvature estimation. *Computer Vision, Graphics and Image Processing: Image Understanding* **55**(1) (1992) 14–26
11. Hautvast, G. et al.: Automatic contour propagation in cine cardiac magnetic resonance images. *IEEE Trans. Med. Imag.* **25**(11) (2006) 1472–1482